Mihran Tuceryan
tuceryan@acm.org
Department of Computer and Information Science
Indiana University Purdue University Indianapolis (IUPUI)
Indianapolis, IN 46202-05132

Yakup Genc
ygenc@scr.siemens.com

Nassir Navab
navab@scr.siemens.com
Siemens Corporate Research
Imaging and Visualization Department
Princeton, NJ 08540, USA

Single-Point Active Alignment Method (SPAAM) for Optical See-Through HMD Calibration for Augmented Reality

Abstract

Augmented reality (AR) is a technology in which a user's view of the real world is enhanced or augmented with additional information generated from a computer model. To have a working AR system, the see-through display system must be calibrated so that the graphics are properly rendered. The optical see-through systems present an additional challenge because, unlike the video see-through systems, we do not have direct access to the image data to be used in various calibration procedures.

This paper reports on a calibration method we developed for optical see-through head-mounted displays. We first introduce a method for calibrating monocular optical see-through displays (that is, a display for one eye only) and then extend it to stereo optical see-through displays in which the displays for both eyes are calibrated in a single procedure. The method integrates the measurements for the camera and a six-degrees-of-freedom tracker that is attached to the camera to do the calibration. We have used both an off-the-shelf magnetic tracker as well as a vision-based infrared tracker we have built. In the monocular case, the calibration is based on the alignment of image points with a single 3D point in the world coordinate system from various viewpoints. In this method, the user interaction to perform the calibration is extremely easy compared to prior methods, and there is no requirement for keeping the head immobile while performing the calibration. In the stereo calibration case, the user aligns a stereoscopically fused 2D marker, which is perceived in depth, with a single target point in the world whose coordinates are known. As in the monocular case, there is no requirement that the user keep his or her head fixed.

1 Introduction

In a typical AR system, the view of a real scene is augmented by superimposing the computer-generated graphics on this view such that the generated graphics are properly aligned with real-world objects as needed by the application. The graphics are generated from geometric models of both nonexistent (virtual) objects and real objects in the environment. For the graphics and the video to align properly, the pose and optical properties of the real and virtual cameras must be the same. The position and orientation of the real and virtual objects in some world coordinate system must also be known. The locations of the geometric models and virtual cameras within the augmented environment may be modified by moving its real counterpart. This is accomplished by track-

Presence, *Vol. 11, No. 3, June 2002,* 259–276

ing the location of the real objects and using this information to update the corresponding transformations within the virtual world. This tracking capability may also be used to manipulate purely virtual objects (ones with no real counterpart) and to locate real objects in the environment. Once these capabilities have been brought together, real objects and computer-generated graphics may be blended together, thus augmenting a dynamic real scene with information stored and processed on a computer.

For augmented reality to be effective, the real and computer-generated objects must be accurately positioned relative to each other, and properties of certain devices must be accurately specified. This implies that certain measurements, or *calibrations,* need to be made at the start of the system. These calibrations involve measuring the pose of various components such as the trackers, pointers, cameras, and so forth. What needs to be calibrated in an AR system and how easy or difficult it is to accomplish the calibration depends on the architecture of the particular system and what types of components are used.

Two major modes of display determine what types of technical problems arise in AR systems, what the system architecture is, and how these problems are to be solved: video see-through AR systems and optical see-through AR systems. The calibration issues in a video see-through system was described in detail elsewhere (Tuceryan et al., 1995). We define an optical see-through system as the combination of a see-through head-mounted display (HMD) and a human eye. We will call this display and eye combination the *virtual camera* of the AR display system.

In this paper, we look at the calibration issues in an AR system of the second type, namely, an optical see-through system. In particular, we concentrate on the camera calibration in both monocular optical see-through displays and stereo optical see-through displays and describe a method of calibration in such a system.

2 Previous Work

Research in augmented reality is a recent but expanding activity. We briefly summarize the research conducted to date in the topic of calibration for augmented reality.

Calibration has been an important aspect of research in augmented reality, as well as in other fields, including robotics and computer vision. Camera calibration, in particular, has been studied extensively in the computer vision community (Maybank & Faugeras, 1992; Weng, Cohen, & Herniou, 1992; Lenz & Tsai, 1988). Its use in computer graphics, however, has been limited. Deering (1992) has explored the methods required to produce accurate, high-resolution, head-tracked stereo display to achieve sub-centimeter virtual-to-physical registration. Azuma and Bishop (1994) and Janin, Mizell, and Caudell (1993) describe techniques for calibrating a see-through HMD. The method of Janin et al. comes closest to our approach in terms of its context and intent, and they consider the tracker in the loop so that the user is free to move during calibration. There are differences between our and their method, however. The first difference is that we use only a single point in the world for calibration, whereas they use a calibration object with multiple points so that the user has to make an extra decision about picking the calibration point and its image. The use of a single calibration point at a time, instead of a multipoint configuration aligned simultaneously, simplifies the user interaction process, which is very important. In the past, we also have implemented interactive calibration schemes that require the simultaneous alignment of multipoint configurations to perform the camera calibration (McGarrity & Tuceryan, 1999). We have found that this makes the user interaction during the calibration process very cumbersome. The second difference between our methods is that they use the traditional intrinsic and extrinsic camera parameterization to model the virtual camera. This requires that a set of nonlinear equations be solved to get the calibration results. We use a projection matrix representation to model the camera which can be estimated by linear methods, making the result of the calibration more robust. We do not need to extract anything more than the projection matrix because ultimately what we want to do is project the 3D objects onto the image plane. The projection matrix has also been found to be more accurate and less sensitive to data collection errors (Navab et al., 1998). Recently, Kato and Billinghurst (1999) described an interactive camera calibration method that uses multiple points on a grid.

Gottschalk and Hughes (1993) present a method for autocalibrating tracking equipment used in AR and VR.

Some researchers have studied the calibration issues relevant to HMDs (Bajura, Fuchs, & Ohbuchi, 1992; Caudell & Mizell, 1992; Azuma & Bishop, 1994; Holloway, 1994, 1997; Kancherla, Rolland, Wright, & Burdea, 1995). Others have focused on monitor-based approaches (Tuceryan et al., 1995; Betting, Feldmar, Ayache, & Devernay, 1995; Grimson et al., 1995; Henri et al., 1995; Mellor, 1995; Peria et al., 1995; Uenohara & Kanade, 1995). Both approaches can be suitable depending on the demands of the particular application.

Various tracking modalities (besides the magnetic trackers) have been used by numerous researchers. Among those, vision-based trackers that use fiducials have been implemented (Koller et al., 1997; Neumann & Cho, 1996; Sauer et al., 2000). Some researchers have also tried to improve the robustness and accuracy of these trackers using hybrid methods (State, Hirota, Chen, Garrett, & Livingston, 1996).

Kutulakos and Vallino (1996) have taken a different approach and demonstrated a calibration-free AR system. These uncalibrated systems work in contexts in which using metric information is not necessary, and the results are valid only up to a scale factor.

3 Overview of the Hardware and Software

To provide the proper context in which to describe our calibration method, and also for the sake of completeness, we briefly review the hardware and software setup. The typical optical see-through AR system hardware is illustrated in figure 1. In this configuration, the display consists of a pair of see-through HMDs. In our setup, we use the i-glasses that can be used both as immersive displays as well as see-through displays by removing a piece of opaque plastic from the front of the display screens. Because our research involves augmented reality systems, we have been using these HMDs as see-through displays permanently. The graphical image is generated by the workstation graphics hardware and displayed on the workstation's monitor, which is fed at the same time to the see-through displays (i-glasses) over a VGA port. This setup also works for other, possibly higher-resolution displays, such as the Sony Glastron or the Microvision VRD. The tracker can be any system that is capable of providing six degrees of freedom (three positional and three rotational). For the work reported in this paper, we have used both a six-degrees-of-freedom (six-DOF) magnetic tracker (Flock of Birds from Ascension Technologies) and an infrared vision-based tracker that we have built ourselves. The tracker provides the workstation with continually updated values for the position and orientation of the tracked objects, which includes the i-glasses and a 3D mouse pointing device.

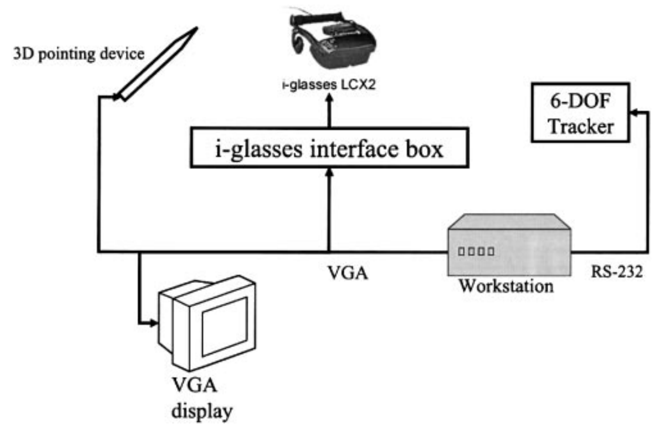

Figure 1. *The hardware diagram of a typical see-through augmented reality system. The particular see-through displays we used for this research are from i-glasses, and have a limited resolution (640×480 for each eye in monocular mode and 640×240 for each eye in stereo mode). We have also experimented with other displays such as the Sony Glastron and the Microvision VRD.*

The software is based on the Grasp system that was developed at ECRC for the purposes of writing AR applications. We have added the calibration capabilities to the Grasp software and tested our methods in this environment. The Grasp software was implemented using the C++ programming language.

4 Overview of the Calibration Requirements

An AR system has both "real" entities in the user's environment and virtual entities. Calibration is the process

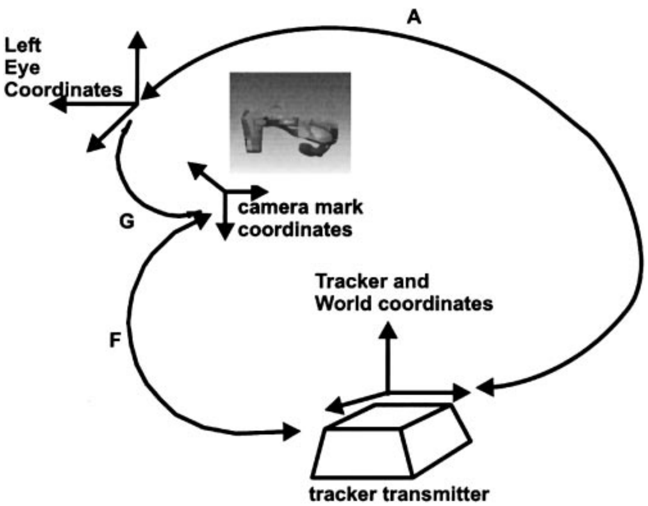

Figure 2. *A simplified version of the coordinate systems that are relevant for the camera calibration of optical see-through systems. The figure shows the coordinate system for only one eye. This is sufficient for the monocular AR system in which the user sees the graphics through only one eye.*

of instantiating parameter values for mathematical models that map the physical environment to internal representations so that the computer's internal model matches the physical world. These parameters may be the optical characteristics of a physical camera as well as position and orientation (pose) information of various entities such as the camera, the magnetic trackers, and the various objects.

The calibration requirements of a video see-through AR system have been described elsewhere (Tuceryan et al., 1995). In this paper, we describe these requirements as modified for an optical see-through system. This modification for an optical see-through system is the new content of this paper that distinguishes it from Tuceryan et al. (1995). Figure 2 shows the local coordinate systems that are relevant for camera calibration in a typical optical see-through AR system. All the calibration requirements for such a system originate from the fact that all the transformations shown must be known during the operation of the AR system. Some of these transformations are directly read from sensors such as the six-DOF trackers, whereas others need to be estimated through a calibration process.

These coordinate systems are related to each other by a set of rigid transformations. The central reference is the world coordinate system (WCS) which is at a fixed and known location relative to the operating environment. During the operation of an AR system, all of the components need to operate in a unified framework, which in the case of the Grasp system is the WCS. For the sake of simplicity in this paper, we have shown in figure 2 the tracker and world coordinate systems as being the same. This allows us to avoid additional calibration issues that are not relevant for this paper. (For a more detailed look at these issues, see Tuceryan et al. (1995).)

In this simplified diagram, the tracker transformation F is read directly from the sensor (called *mark*) attached to the HMD. For the monocular case reported in this paper, we use only one eye to display the graphics. The display for the other eye is covered so that the AR display is truly monocular. The transformation G from the mark to one eye is not known and needs to be calibrated. The transformation A that models the camera with respect to the WCS is inferred from F and G.

Camera calibration is the process by which the extrinsic camera parameters (location and orientation) as well as the intrinsic camera parameters (focal length, image center, and aspect ratio) are calculated for a given camera. Normally, this process would calculate the transformation labeled A in figure 2 as well as the camera intrinsic parameters. In the case of a video see-through camera calibration system, this would be the estimation of the parameters for the physical camera. In the case of an optical see-through AR system, estimating A directly would require that we collect a sufficient number of 3D–2D point correspondences without moving the head and body in the process. Because this is an almost impossible task, we choose to calibrate G (which is fixed because the tracker sensor is rigidly attached to the HMD) and infer A from G and F. The resulting calibration parameters describe a virtual camera that models the combined imaging system formed by the i-glasses display and the human eye.

A point in the world coordinate system P_W is projected on the image plane of the virtual camera as P_I with

$$\rho P_I = AP_W = GFP_W, \qquad (1)$$

where G is the projection matrix from tracker mark coordinate frame to the virtual image plane and ρ is a scalar.

5 Camera Calibration for Optical See-Through Displays

In this section, we will describe our calibration method for an optical see-through HMD. After some preliminaries in subsection 5.1, we describe our calibration method for monocular optical see-through HMDs in subsection 5.2. Then, we will extend it to the stereo display case in subsection 5.3. The camera calibration method described in our previous work on video see-through systems was based on using the correspondence between known 3D points and the 2D positions of their projected image positions. From this, the camera parameters were estimated (Tuceryan et al., 1995). This was purely for the video see-through case in which it was assumed that we have access to the picture points (pixels), which we can select and whose image coordinates we can obtain. This can be done in a video see-through display system because we can always access the image digitized by the video camera and use it to analyze the input images. With an optical see-through system, the images of the scene are formed on the retina of the human user's eye and we do not have direct access to the image pixels. Therefore, we need to have a different approach to calibrating optical see-through systems.

The most difficult part of calibrating such a system is devising the proper user interaction method for collecting the necessary data for performing the calibration. There have been attempts in the past to devise such interaction methods with various degrees of success. The earlier methods tried to use multiple-point configurations in the world to collect the calibration data. Examples of this include the method of Janin et al. (1993). Another approach in the past has been to have the user align a model of a 3D object with multiple configurations with the physical object in the display interactively. In an earlier paper, we described such an interactive approach for calibrating an optical see-through AR system (McGarrity & Tuceryan, 1999). That approach let the user adjust camera parameters interactively until he or she was satisfied that a 3D model of a calibration jig was aligned properly with the physical calibration jig itself. This method worked, but the user interface was cumbersome. The major advantage of using a single point at a time makes the alignment process during calibration a much easier task for the user. Notice also that the fact that we are aligning a single point at a time does not preclude us from using multiple calibration points (although we have not implemented this), but only that we need to use them one at a time. In fact, using multiple calibration points may be one way to extend the method presented in this paper to calibrate for trackers that extend over a large area. In addition, the number of parameters being estimated was too large, and, therefore, the interaction did not provide a very intuitive feedback to the user. In general, we have found that using multipoint configurations and demanding that the user align them simultaneously or use them to collect data in some fashion is cumbersome and prone to errors.

The contribution of the method described in this paper is an attempt at making this interaction easy for the user and reduce the causes of error by making the user's task for collecting data simple. The approach described in this paper has two major advantages compared to previous approaches. First, it simplifies the data collection process by making the interaction very simple: aligning a single cursor with a single point in the world. This is in contrast to the traditional camera calibration approaches that have access to pixel data in a video buffer or to previous interactive approaches in which the user is either required to keep his or her head from moving while collecting data or the user is asked to interactively align a multiple-point configuration simultaneously. Second, because we keep the camera model as a projection matrix without decomposing it into its intrinsic and extrinsic components, the results are numerically more stable.

The user interaction needed to collect the data for the calibration is a streamlined process and does not impose a great burden on the user. During this process of aligning a single cursor on the display with a single world point, there is no interaction with a mouse or any other device to try to move items on the display at the same time that the head is moving. These types of multiple task interactions increase the complexity and make the calibration process more cumbersome and prone to error (McGarrity & Tuceryan, 1999). Therefore, a major source of errors as well as a source of difficulty in interaction is eliminated by keeping the user interaction simple in the calibration procedure.

In the following subsections, we first briefly describe the camera model we are using, which defines the parameters to be estimated. We then describe the calibration procedure for both the monocular and the stereo displays.

5.1 Camera Model and Calibration Formulation

A simple pinhole model is used for the camera, which defines the basic projective imaging geometry with which the 3D objects are projected onto the 2D image surface. The coordinate systems can be set up in different ways, and, in our model, we use a right-handed coordinate system in which the center of projection is at the origin and the image plane is at a distance, f (focal length), away from it.

A pinhole camera can be modeled by a set of intrinsic and extrinsic parameters. The intrinsic parameters are those that define the optical properties of the camera such as the focal length, the aspect ratio of the pixels, and the location of the image center at which the optical axis intersects the image plane. One last intrinsic parameter is the skew of the image plane axes. The intrinsic parameters are usually modeled by a 3×3 matrix of the form

$$\prod = \begin{bmatrix} f_u & \tau & r_0 \\ 0 & f_v & c_0 \\ 0 & 0 & 1 \end{bmatrix} \qquad (2)$$

where f_u and f_v are the focal lengths in the directions of two major axes in the image plane, (r_0, c_0) is the location of the image center, and τ describes the skew between the two axes in the image plane. The f_u and f_v also model the scale factor and aspect ratio in going from the sensor units to image units. The 3D points in the world coordinate system get projected onto the image plane of the camera to form the image points.

The extrinsic parameters define the position and orientation (pose) of the camera with respect to some external world coordinate system and are given by a 3×3 rotation matrix R and a 3×1 translation vector T.

The camera transformation that maps 3D world points into 2D image coordinates can be characterized by writing the transformation matrices for the rigid transform defining the camera pose and the projection matrix defining the image formation process. This is given by the classic equation

$$\rho \mathrm{P}_I = \prod[\mathrm{R}\ \mathrm{T}]\mathrm{P}_W \qquad (3)$$

where $\mathrm{P}_W = [x_W, y_W, z_W, 1]^T$ is the homogeneous 3D coordinates of the world point and $\mathrm{P}_I = [x_I, y_I, 1]^T$ is the homogeneous coordinates of its image. The overall camera transformation, therefore, is a 3×4 matrix

$$\mathrm{T}_{camera} = \prod[\mathrm{R}\ \mathrm{T}] \qquad (4)$$

The entries of T_{camera} can be estimated directly instead of the actual extrinsic and intrinsic camera parameters. This estimation is a standard technique that is often used in computer vision. The calibration proceeds by collecting a number of 2D image coordinates of known 3D calibration points, and the correspondence between the 3D and 2D coordinates defines a linear system to be solved in terms of the entries of the camera matrix. (See appendix A.)

Normally, in traditional video cameras, this 3D–2D correspondence is done by identifying the calibration points in a statically grabbed image of a calibration jig. In an optical see-through display, collecting these correspondences in a similar way would require that the HMD and the user's head (and body) be fixed. Because this is not realistic, we have modified the data collection process so that the user does not have to keep his or her head and body fixed.

5.2 Calibration Procedure for the Monocular Case

To get a practical calibration procedure for the see-through displays, the preceding formulation needs to be converted to a user-friendly procedure. This means that the design of the way in which the calibration data is collected by the user has to be thought out carefully to minimize the burden on the user and the chances of making errors.

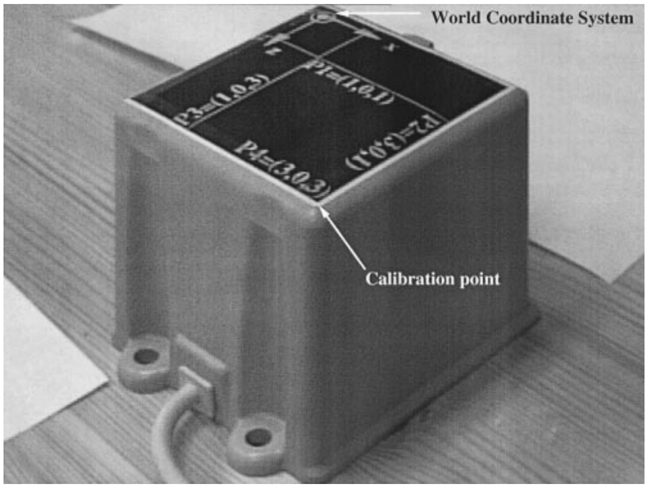

Figure 3. *The world coordinate system is fixed on the tracker transmitter box as shown in this image.*

In our method, we have a tracking system that is attached to the HMD in a rigid way. The tracker can be anything that provides six-DOF positional and rotational data. We have used both a magnetic tracker and an infrared vision-based tracker that we built. In our discussion in this paper, we will normally refer to the magnetic tracker. The tracker system can read (sense) the position and orientation of the receiver in the tracker coordinate system. For convenience, we call the tracker sensor attached to the HMD (the object to be tracked) the *mark*. Because the mark is attached rigidly to the HMD, the camera can be defined and calibrated with respect to the mark coordinate system. Therefore, taking this approach, we have the camera transformation fixed and unaffected by the head motion. This is the reason that the head is allowed to move freely during our calibration procedure.

Referring to figure 2, we see three coordinate systems that are relevant for the monocular camera calibration, and the transformations between them (A, F, and G). The transformation A is the 3×4 projective camera transformation with respect to the world coordinate system that is estimated in traditional video-based systems, and F is a 4×4 homogeneous transformation matrix that defines the tracker mark position and orientation being sensed and updated. Finally, G is the 3×4 projection matrix that defines the camera transformation with respect to the mark coordinates.

To calibrate the camera (that is, to estimate the transformation A), we need to get the image coordinates of known 3D points in the world coordinate system, but A is not fixed and varies as the user moves his or her head. Therefore, we obtain A indirectly by estimating the transformation G which does not change, and computing A = GF.

Thus, the camera calibration for such a system means we need to estimate the transform G. We have implemented the calibration procedure as follows.

1. A single point in the world coordinate system (see figure 3) is used to collect the calibration data. This single point in the world coordinate system is mapped to many distinct points in the mark coordinate system as the user's head (and body) is moved about. This is given by the formula $P_M = FP_W$. Because F is changing as the head moves, so is, therefore, the coordinates of the point P_M in the mark coordinate system even though P_W is fixed.
2. The user is presented with a 2D marker[1] on the display and is asked to move his or her head and body until the marker is aligned with the image of the single calibration point as seen by the user. (See figure 4.) The user then clicks a button on the 3D mouse and the data is collected for calibration that consists of the image coordinates of the 2D marker, P_I, and the 3D coordinates of the calibration point in mark coordinates, P_M. These collected points are then fed into the equation (7) (in appendix A), which is used to estimate the transformation G. After the matrix G is estimated, it is integrated in Grasp and OpenGL as described in appendix B so that the graphics are rendered correctly.

1. We use the term *marker* generically both here and in subsection 5.4 to indicate a 2D marker on the display that the user aligns with the calibration point in the world. The shape of this marker becomes important, particularly in the case of the stereo calibration procedure, to improve the perception of alignment in depth. (See Section 6 for details.)

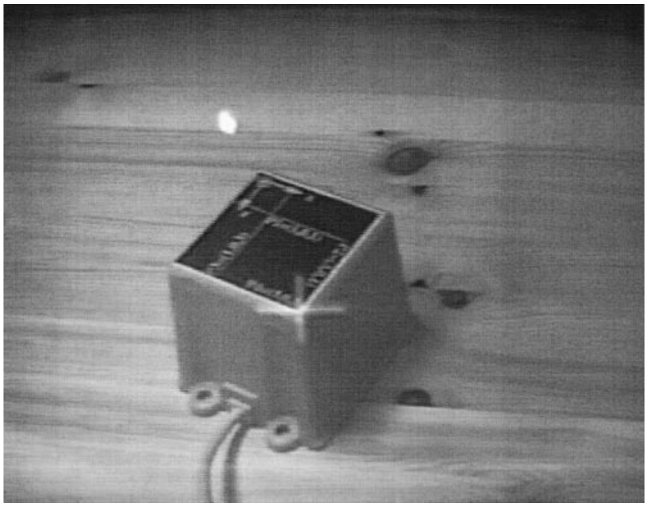

Figure 4. *The calibration procedure requires the user to align a cursor as shown here with a fixed point in the world.*

Normally, we need to collect a minimum of six points for the calibration. However, to account for the errors and obtain a more robust result, we collect more points and use a least squares estimation as stated in appendix A. Notice here that the more of the tracker volume that the user's head covers, the more possible systematic errors in the tracker measurements will be taken into account in the optimization process. The user is encouraged to move his or her head around the tracker transmitter as much as possible while collecting the calibration data. It is not always easy for the user to cover all possible angles during the calibration. For example, it is easier for the user to move around the calibration point sideways than trying to obtain top views. The important thing is to perform the calibration from the set of viewpoints that the user will use during the operation of the AR system. Another restriction on the user's movements during calibration is that, if the tracker being used has any intrinsic range restrictions, naturally, the user will be restricted to those areas. For example, most of the popular magnetic trackers have range restrictions from 3 ft. to 10 ft. In this case also, the user is encouraged to cover as much of the volume that is going to be actually used. In the monocular case, we have implemented the 2D marker as a crosshair centered on the pixel, and its components have odd-numbered widths. The resolution of the marker is limited by the resolution of the display and clearly this can have an effect on the accuracy of the result. However, even more important is how the user actually aligns this cursor with the calibration point. Even if we tried to design the marker with great resolution, we would still have no control over how the user aligns it during calibration. The inaccuracies in the tracker measurements and user's alignment are greater sources of error than is the resolution of the cursor.

5.3 Calibration Formulation for Stereoscopic Displays

Although the extension of the preceding calibration method to stereo HMD displays is straightforward, we still would like to keep the interaction method as simple and as less cumbersome as possible. Therefore, we would like to avoid calibrating the left and right displays independently using the previous method. The stereo calibration method presents a marker to the left and right eyes of the user with a horizontal disparity and relies on the human visual system's ability to fuse left and right views of a cursor to generate a marker in depth. This perceived marker in depth is then aligned by the user with the target calibration point in the WCS. The use of stereoscopic perception to make precise alignments is a complicated issue that has been studied by other researchers. For example, Nagata (1991) has studied the depth sensitivities of visual cues such as binocular parallax, motion parallax, and accomodation. He has found in this work that "of the different cues, binocular parallax is most effective at distances of less than 1 m." In most situations, the working volume for the methods described in this paper are within this range. We also address the perception of depth and depth accuracy later in the paper.

The camera model and the mathematics of the calibration are the same as the monocular case just presented, but now there are two displays (a left one and a right one). The stereo setup is summarized in figure 5, which shows the coordinate systems that are relevant for the calibration of a stereo optical see-through system. In this figure, we see five transformations (A_L, A_R, F, G_L, and G_R) that need to be estimated. The transformations

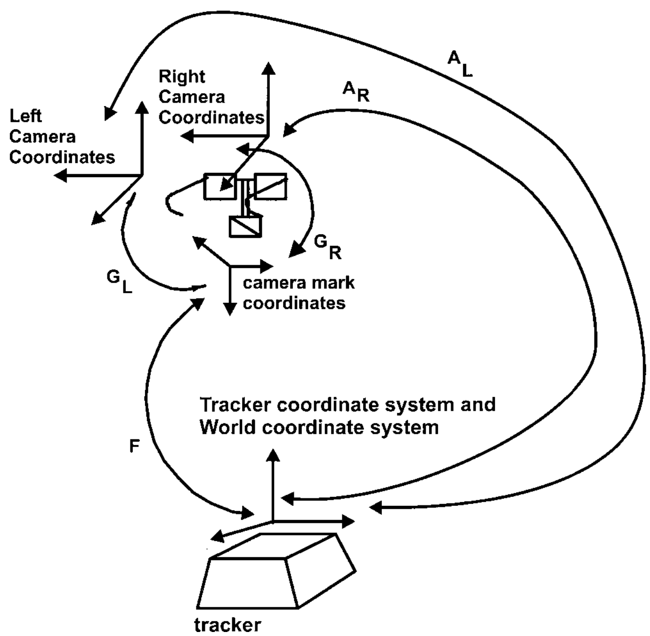

Figure 5. *Figure 2 modified to show the coordinate systems in a stereo optical see-through setting.*

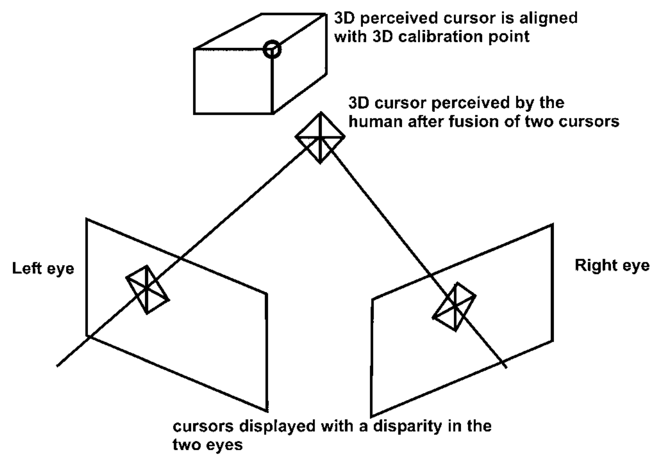

Figure 6. *The data collection by the user for calibrating the display is performed by the user moving his head until the perceived crosshair in 3D is colocated with the 3D calibration point.*

A_L and A_R are the traditional 3×4 projective camera transformation with respect to the WCS. Similarly, F is a 4×4 homogeneous transformation matrix that defines the tracker to mark rigid transform. That is, F is the pose of the mark with respect to the tracker transmitter coordinate system. Finally, G_L and G_R are the 3×4 projection matrices that define the camera transformations with respect to the mark coordinates. As in the monocular case, for simplicity we assume that the tracker and world coordinate systems are the same. The figure can be summarized by two equations:

$$A_L = G_L F$$
$$A_R = G_R F. \qquad (5)$$

The calibration data is collected as a set of 3D–2D point correspondences that are then used to solve for the camera matrices G_L and G_R. The contribution of this part of the paper comes in collecting the calibration data for both eyes in a single step.

5.4 Calibration Procedure for Stereoscopic Displays

The data collection procedure for calibrating the stereo displays is as follows.

1. A single point in the world coordinate system is used to collect the calibration data. This single point in the WCS is mapped to many distinct points in the mark coordinate system as the user's head moves. This is given by the formula $P_M = FP_W$. Because F is changing as the head moves, so is, therefore, the coordinates of the point, P_M, in the mark coordinate system even though P_W is fixed.
2. The user is presented with 2D markers on the display for each eye placed randomly in the 2D image plane. The markers for the two eyes are slightly offset, creating a disparity. The user's brain automatically fuses these markers, and the user perceives it in three dimensions at a particular location in depth. The user collects the calibration data by moving his or her head and body until he aligns the perceived marker in 3D with the 3D physical calibration point. (See figure 6.) The user then clicks a button on the 3D mouse, and the data is collected for calibration that consists of the image coordinates P_I of the 2D marker and the 3D mark coordinates P_M of the calibration point.

These collected points are now used to estimate the camera matrices as described in appendix A. As in the monocular case, the user is encouraged to cover as much of the tracker volume that will be used during the operation of the AR system.

Because we do not know what the camera geometry is before the calibration is actually performed, we do not have a rigorous way of determining what the disparities should be for the image markers in the left and right eyes. However, we have some rough idea about what the depth range should be. This is determined either by the range restrictions of some trackers or by the fact that, as the distance in depth of the marker from the user increases, the depth acuity of the user decreases and alignment becomes more difficult. With these restrictions in mind, we picked the disparities in a range that, when the HMDs were worn, the marker in depth was roughly within arm's length and within the tracker range. This was done by trial and error. Notice that we do not need to compute the actual depth of the marker, and the values of the disparities are inputs to the calibration procedure. As long as the disparities result in a fused marker in depth that is reasonably easy to align in depth, we have the calibration procedure set. The disparities are also varied for the various markers presented to the user during the data collection process.

Because we have 2D positions of the markers for both eyes when the mouse is clicked and because the user has aligned the 3D crosshair with the 3D world point, this is equivalent to having the two markers in the two eyes aligned with the corresponding images of the world point. Therefore, at the moment that the mouse button is clicked, calibration data in the form of P_I and P_M is collected for both left and right eyes simultaneously. In particular, we have the crosshair position $P_{I,L}$ for the left eye and $P_{I,R}$ for the right eye, where $P_{I,L} = P_{I,R}$ + disparity. The world point position in mark coordinates is the same for both eyes (because we have a single mark attached to the entire goggles which is moving rigidly). Therefore, these data can now be used to estimate the camera parameters for both the left and the right eyes independently.

Notice that we do not make any assumption that the result of the calibration will be the same for different users. In fact, the fact that the camera matrices G_L and G_R are estimated for each user means that we are not assuming that they are the same for different users. Also, this means that variations in interocular distances and any differences in depth perceptions will be accounted by the camera matrices estimated for each user.

After the projection matrices are estimated for the left and right eyes (cameras), they are integrated in Grasp and OpenGL as described in appendix B.

6 Experimental Verification for Calibration

A serious problem with the verification of an optical see-through display calibration is that it is not possible to show how well the model corresponds with the object for a human viewer. This is a difficult task for the monocular displays, but it gets even more difficult to show quantitative results for the stereoscopic displays.

This problem can be approached in a number of ways, from simple to more complex. The first and simplest approach to either type of display is to have a human put the HMDs on, go through the calibration procedure, and report whether the result is "good" or "bad." We have used this approach with a number of users. In fact, we did set up demo sessions at the International Workshop on Augmented Reality (IWAR '99) and at the International Symposium on Augmented Reality (ISAR '00) at which many users tried the calibration scheme within the live demo setting. The results of these trials were generally positive. Many users who tried the calibration were satisfied with the resulting accuracy of the calibration. However, we have no way of reporting any objective data on these experiments.

A second and more complicated approach is to replace the human eye with a video camera in some fashion in the optical see-through displays and apply the calibration method via this camera (with the displays). This allows us to obtain video images of the procedure as well as the results.

We have built a setup in which a camera is put in a mannequin's head behind the i-glasses displays and the display is recorded. (See figure 7.) The images in figures

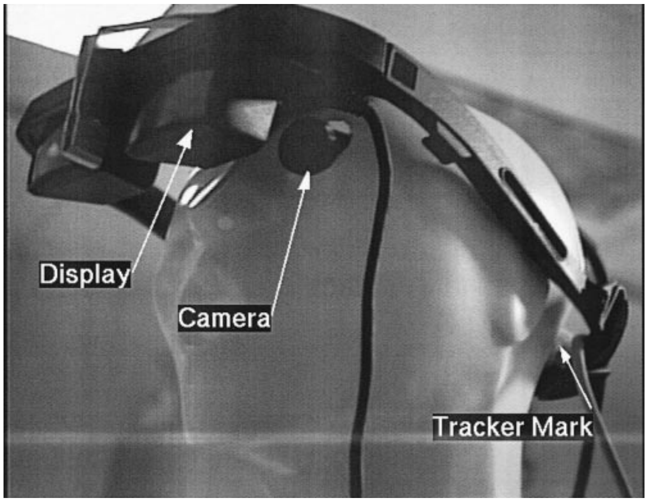

Figure 7. *A mannequin's head with a camera placed at the eye behind the i-glasses displays. This setup was built so that we could collect images during and after the calibration of the HMD.*

Figure 9. *A lamp is being placed in the scene by using the tip of the pointer to indicate the location. This type of interaction works properly because both the display and the pointer are properly calibrated.*

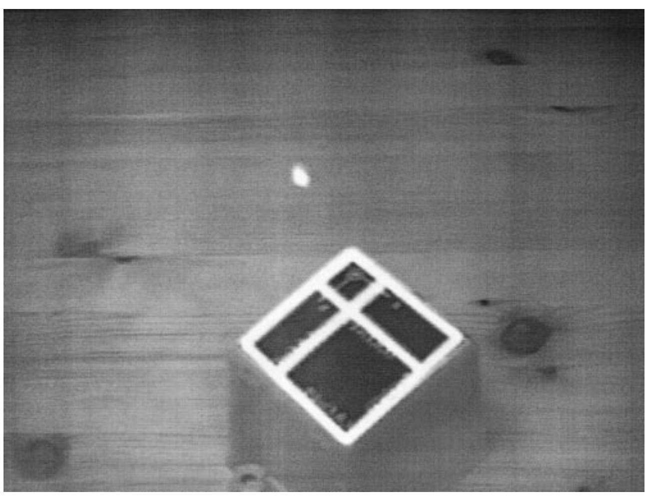

Figure 8. *An image captured from the camera in the mannequin's head showing the aligned model of the world coordinate axes with their physical locations.*

4, 8, and 9 were collected using this setup. Figure 4 shows the view of the user during the monocular calibration in which the cursor is aligned with the world point in the display. A sample result of the monocular calibration is shown in figure 8 in which a model of the calibration pattern defining the world coordinate axes is shown superimposed on the image of the real tracker with the WCS on it. We have tried this calibration method in numerous trials, and in all instances the calibration results are very good. The quality of the alignment shown in figure 8 is representative of the calibration results in these trials. The quality of the calibration results does not change greatly as the head moves around in the world. The only problem is due to the lag in the readings from the magnetic tracker, which tends to settle down to the correct position after a certain delay after the head stops moving.

In the case of using magnetic trackers, some of the factors that affect the calibration include the distance of the user's head from the tracker transmitter and how quickly the user clicks the mouse to collect the calibration data. The magnetic tracker we use has a range of approximately 3 ft., and the quality of the sensor readings are not very reliable when the receivers operate near the boundaries of this range. The problems arising from this can be alleviated if an extended-range tracker is used that has a larger operational volume (approximately 10 ft.). The second factor that affects the calibration is the lag in the tracker data at the point of collection (that is, when the mouse is clicked). If the button is clicked too quickly, the tracker data read may not correspond to the location of the user's head. We have found that, if the user is careful during the calibration, both of these factors can be put under control and the calibration results are good.

A third way in which we can try to quantify the accuracy of our results of calibration is to use a video see-through setup and calibrate it using the method described in this paper. This does not exactly match the conditions and optics of the optical see-through displays, but it approximates them. In the process, it also allows us to capture the event on video and later analyze the accuracy of the results. Therefore, we have also implemented the calibration procedure described in this paper in a video see-through system.

The video see-through system we have used is developed and described in detail by Sauer et al. (2000). Here, we review this system briefly for the sake of completeness, keeping in mind that this paper is not about the RAMP system, which is based on a Kaiser ProView XL35 HMD. Two Panasonic GP-KS1000 color cameras provide the stereo images, and a black-and-white Sony XC-77RR with a wide-angle lens is used for tracking. Two SGI visual PCs, one 320 and one 540, process the three video streams. The system runs in real time at a framerate of thirty frames per second and exhibits a low latency of only about two frames. The software was developed under Windows NT and now runs under Windows 2000.

As we mentioned in subsection 5.2, our experiments showed that, in the case of stereo calibration in which depth perception is important, the choice of the display marker shape was important. We first used a marker shaped like a crosshair (as in the monocular calibration) to align with a surface mark in the scene. However, unlike the monocular case, the crosshair shape did not provide enough visual cues in the stereo calibration for the user to accurately align it with the calibration point in depth. We tried other marker shapes, and the more-successful shapes turned out to give the perception of a plane with an orientation as well as the depth. So, for example, a solid disk or a rhombus shape with a cross inside it worked better. Having the plane of the marker pointing in a certain direction as the user moved towards the calibration point made the alignment in depth a little easier. We discovered that the user could improve this accuracy by moving back and forth in depth to see when the calibration point was crossing the plane of the marker.

One of the most important issues we were interested in addressing was to determine the degree of accuracy of the stereo alignment process previously described. Because our video see-through system provided us with the complete tracking and calibration parameters, we conducted the following experiment to assess the accuracy of the alignment process. We first set the disparity between the left and right images of the virtual marker such that it is at some distance away from the user. Using the calibration parameters obtained for the two cameras providing the stereo image stream for the HMD, we computed the position of the virtual object in the tracker coordinate system. We then let the users do the alignment from different positions for the same disparity many times. With a fixed disparity, the users can move their heads on a sphere centered at the physical target. Therefore, when the virtual marker and the physical target are aligned, the different positions of the user's head should be at the same distance to the physical target. We recorded some 15 to 35 such alignments per user for two different disparity values (resulting in marker distance of 750 mm and 720 mm). We found in each case that these alignments resulted in an average distance very close to the measured ones with a standard deviation of around 1 mm or better. Figure 10 shows the results of multiple trials of depth alignment for a typical user. As can be observed from the graph, the alignment is very consistent over the trials for the particular user. We have also tried for other users, and the results are comparable to this example.

We also conducted some experiments to assess the reprojection errors for the estimated projection matrices. The results are presented in figure 11, which shows the results for two experiments on one user. The experiments were run for three different users, and the results from the other users are comparable to the results in this figure. Figure 11(a) shows the reprojection errors in the left image of the perceived 3D point picked by the user (that is, the cursor is aligned with the target point), and figure 11(b) shows the reprojection errors in the right image for the same data. Each point in this figure represents one of the data points collected. As can be seen from the data, the uncertainty in the horizontal

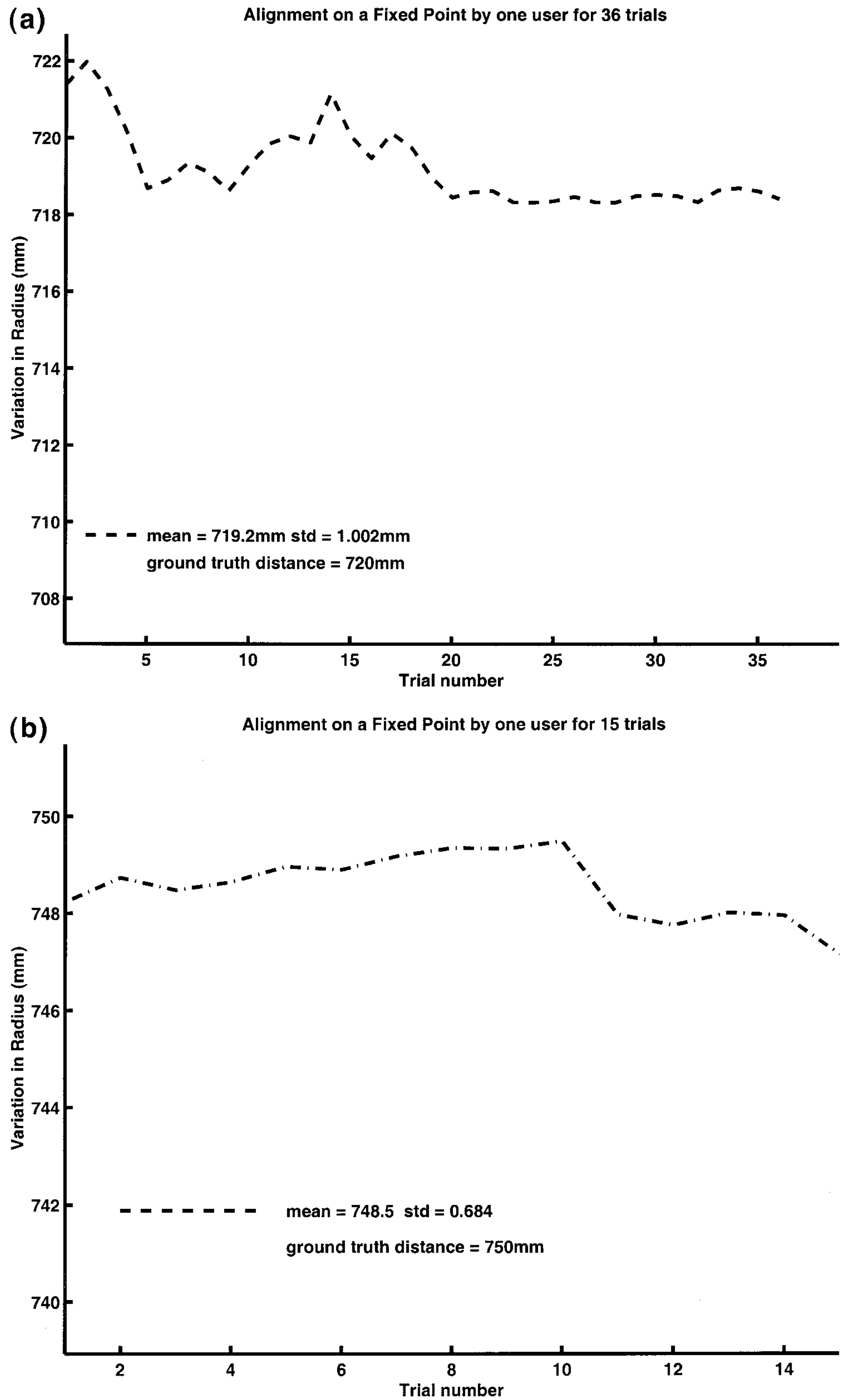

Figure 10. *Experimental results of measuring the accuracy of the depth judgment for the perceived marker. (a) shows the alignment results for the ground truth distance of 720 mm over 36 trials (x axis) for one of the users, and (b) shows the alignment results for the ground truth distance of 750 mm over 15 trials for the same user.*

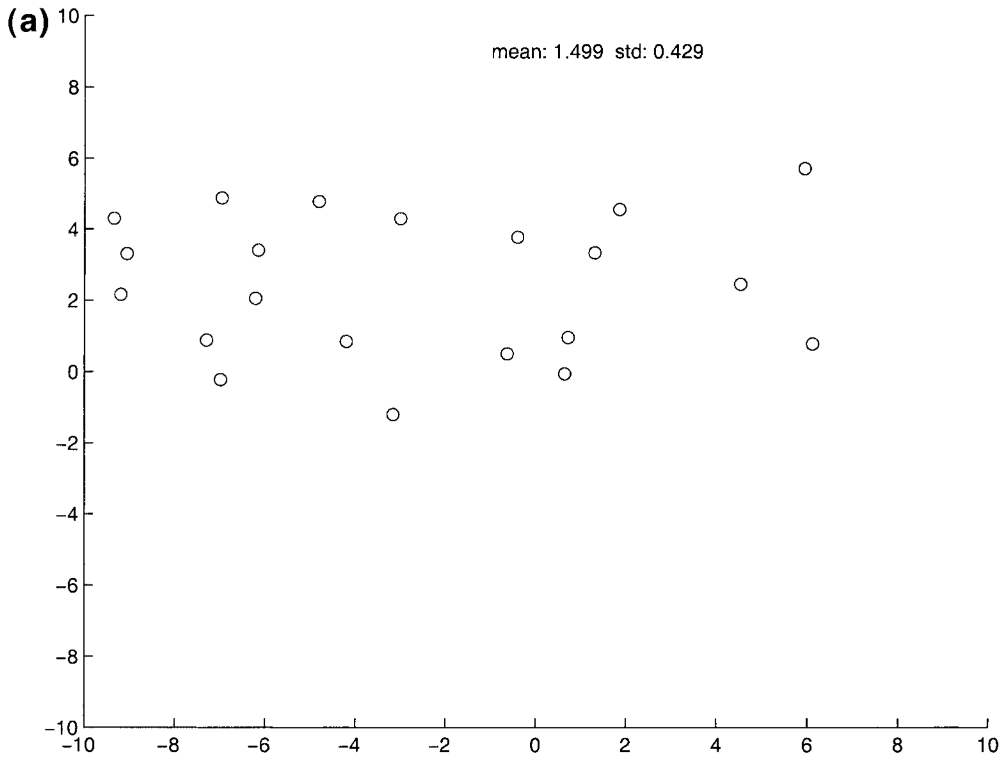

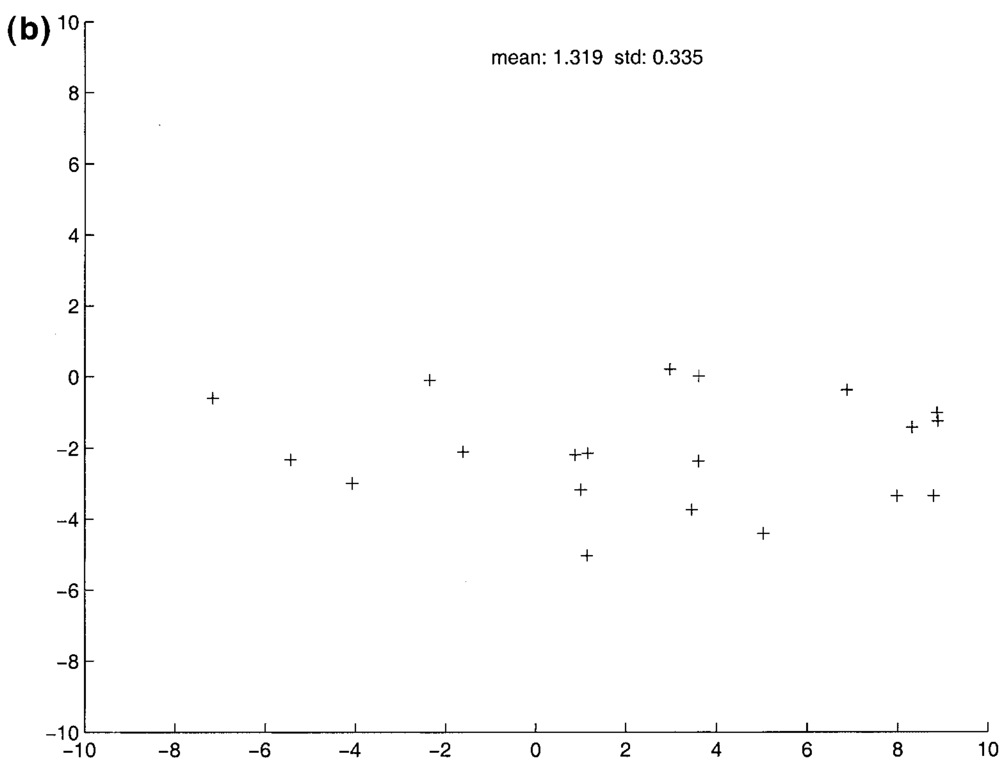

Figure 11. *The 2D error distribution of the projection (perceived) point. (a) The distribution for the left image, and (b) for the right image.*

direction is larger than in the vertical direction. This is not surprising because the depth perception depends on the horizontal disparity in our setup. The mean error for the left image is 1.499 pixels with a standard deviation of 0.429. For the right image, the mean reprojection error is 1.319 pixels with a standard deviation of 0.335. The results are similar for the other users not shown in this figure. As can be seen from this figure, the reprojection errors are quite low, less than 1.5 pixels on the average.

7 Conclusion

In this paper, we presented a camera calibration procedure for optical see-through HMDs for AR systems. Because in optical see-through AR systems we do not have direct access to the image produced on the retina, the procedure needs to use indirect methods to do the calibration. The method presented in this paper uses an interactive method to collect calibration data, and it does not require that the user keep his or her head still. The method presented works for calibration of monocular as well as stereoscopic optical see-through HMDs. The method uses a very simple interaction method to collect the 3D–2D point correspondences needed to compute the camera parameters. The user's head is not required to be immobile during the data collection process, and the method can be extended to larger areas with multiple calibration target points as long as they can be selected one at a time. The user is encouraged to cover during calibration as much of the target operating volume as possible to account for tracker errors.

The paper also reports some experimental methods and results that attempt to measure the accuracy of the resulting calibrations objectively. Future research efforts need to improve these assessment and evaluation methods for optical see-through systems.

Appendix A Standard Camera Calibration Formulation

The standard projective camera calibration is set up as follows. Let there be n calibration points whose image coordinates we measure. We need to estimate twelve parameters of the 3×4 projection matrix, but the projection matrix is defined up to a scale factor. Therefore, really only eleven independent parameters need to be estimated. Therefore, n, the number of calibration points to be measured, should be at least six. However, to make the calibration results more robust against noise and user errors, normally more data points are collected and the estimation is done using a least squares approach.

Let the ith measurement point have homogeneous mark coordinates $P_{M,i} = [x_{M,i}, y_{M,i}, z_{M,i}, 1]^T$ and its image point have homogeneous image coordinates $P_{I,i} = [x_i, y_i, 1]^T$. The basic camera equation is given by

$$\rho \mathrm{P}_{I,i} = \mathrm{G}\mathrm{P}_{M,i} \quad \text{for } i = 1, \cdots, n. \tag{6}$$

This gives us a linear equation to solve for the entries of the 3×4 camera matrix G:

$$\mathrm{Bp} = 0, \tag{7}$$

in which p is the unknown parameter vector that consists of all the entries $[g_{ij}]$ of the G matrix put into a column vector. The coefficient matrix B is given by

$$\mathrm{B} = \begin{bmatrix} \vdots & \vdots & \vdots & \vdots & \vdots & \vdots & \vdots & \vdots & \vdots & \vdots & \vdots & \vdots \\ x_{M,i} & y_{M,i} & z_{M,i} & 1 & 0 & 0 & 0 & 0 & -x_i x_{M,i} & -x_i y_{M,i} & -x_i z_{M,i} & -x_i \\ 0 & 0 & 0 & 0 & x_{M,i} & y_{M,i} & z_{M,i} & 1 & -y_i x_{M,i} & -y_i y_{M,i} & -y_i z_{M,i} & -y_i \\ \vdots & \vdots & \vdots & \vdots & \vdots & \vdots & \vdots & \vdots & \vdots & \vdots & \vdots & \vdots \end{bmatrix}. \tag{8}$$

The matrix B has $2n$ rows, two rows for each data point, and twelve columns. If more than six points are collected, the system is overdetermined.

Solving this equation gives us the camera matrix G. As we mentioned before, there are only eleven independent parameters and the camera equation is valid up to a scale factor. Therefore, to solve the camera equation (7), we estimate the unknown parameter vector p by minimizing $\|Bp\|^2$ such that $\|p\| = 1$. This puts a constraint on the scale and reduces the number of parameters to eleven. The solution to this constraint minimization is found by finding the eigenvector associated with the smallest eigenvalue (Trucco & Verri, 1998, appendix A). In practice, this is done by finding the singular value decomposition (SVD) of the matrix B given by $B = UDV^T$, and the solution is the column of the matrix V corresponding to the smallest singular value.

Appendix B Integrating the Projection Matrix with OpenGL

Because our camera model now consists of a 3×4 projection matrix, we have to implement the renderer to use a camera defined by a 3×4 projection matrix. Unfortunately, OpenGL does not provide an easy interface to do this, so, we had to write a camera class in C++ that is defined by a projection matrix but that uses a number of OpenGL calls to implement the camera. Even though, the details presented in this section are routine; we believe that giving these details enhances the reproducibility of the results and algorithms presented in this paper by other researchers. Therefore, we give these details for the sake of completeness.

The decision to write a C++ camera class is a result of the fact that all our implementation is done using the GRASP platform developed at ECRC which was written in C++. In fact, the new camera class is implemented as a subclass of the GRASP camera class. In implementing this camera class, we have to be careful that the renderer does not take a performance hit, and that we do not extract explicit intrinsic camera parameters for doing this. So, in our implementation, we set up the viewing transformation as an orthographic projection, but push our own constructed viewing matrix onto the transformation stack.

To accomplish this, we need to create a 4×4 matrix that has the clipping plane information from OpenGL as well as our estimated camera projection matrix entries. So, here are the steps to convert it into an OpenGL viewing matrix. First, we make our 3×4 camera matrix G into a 4×4 matrix which has the depth entries in the third row. This is accomplished by multiplying the camera matrix with the transform

$$\begin{bmatrix} 1 & 0 & 0 \\ 0 & 1 & 0 \\ 0 & 0 & -(f+n) \\ 0 & 0 & 1 \end{bmatrix}. \tag{9}$$

Here, f and n are the far and near clipping planes, respectively, used by OpenGL. In addition to the far and near clipping planes, there are the top (t), bottom (b), left (l), and right (r) clipping planes, which will be used in the following equations.

Next, we add in the entry that is used for z-buffer quantization as defined by the matrix

$$\begin{bmatrix} 0 & 0 & 0 & 0 \\ 0 & 0 & 0 & 0 \\ 0 & 0 & 0 & f \cdot n \\ 0 & 0 & 0 & 0 \end{bmatrix} \tag{10}$$

Next, we define the form of the orthographic projection matrix in OpenGL as defined by the function call $glOrtho(l,r,b,t,n,f)$. This is given by the matrix

$$\begin{bmatrix} 2\ (r-l)^{-1} & 0 & 0 & -\dfrac{r+l}{r-l} \\ 0 & 2\ (t-b)^{-1} & 0 & -\dfrac{t+b}{t-b} \\ 0 & 0 & -2\ (f-n)^{-1} & -\dfrac{f+n}{f-n} \\ 0 & 0 & 0 & 1 \end{bmatrix}.$$

Finally, we obtain the OpenGL viewing matrix by putting all these together as follows:

$$CAM = \left(\begin{bmatrix} 1 & 0 & 0 \\ 0 & 1 & 0 \\ 0 & 0 & -f-n \\ 0 & 0 & 1 \end{bmatrix} G + \begin{bmatrix} 0 & 0 & 0 & 0 \\ 0 & 0 & 0 & 0 \\ 0 & 0 & 0 & fn \\ 0 & 0 & 0 & 0 \end{bmatrix} \right) \times \begin{bmatrix} 2\,(r-l)^{-1} & 0 & 0 & -\dfrac{r+l}{r-l} \\ 0 & 2\,(t-b)^{-1} & 0 & -\dfrac{t+b}{t-b} \\ 0 & 0 & -2\,(f-n)^{-1} & -\dfrac{f+n}{f-n} \\ 0 & 0 & 0 & 1 \end{bmatrix}.$$

References

Azuma, R., & Bishop, G. (1994). Improving static and dynamic registration in an optical see-through display. *Proceedings of the 21st Annual Conference on Computer Graphics,* 197–204.

Bajura, M., Fuchs, H., & Ohbuchi. (1992). Merging virtual objects with the real world: Seeing ultrasound imagery within the patient. *Proceedings of the 19th Annual Conference on Computer Graphics,* 203–210.

Betting, F., Feldmar, J., Ayache, N., & Devernay, F. (1995). A framework for fusing stereo images with volumetric medical images. *Proceedings of the IEEE First International Conference on Computer Vision, Virtual Reality and Robotics in Medicine (CVRMed'95),* 30–39.

Caudell, T., & Mizell, D. (1992). Augmented reality: An application of heads-up display technology to manual manufacturing processes. *Proceedings of the 25th Annual Hawaii International Conference on System Sciences (HICSS-25)*, vol. II., 659–669.

Deering, M. (1992). High resolution virtual reality. *Proceedings of the 19th Annual Conference on Computer Graphics,* 195–202.

Gottschalk, S., & Hughes, J. (1993). Autocalibration for virtual environments tracking hardware. *Proceedings of the 20th Annual Conference on Computer Graphics,* 65–72.

Grimson, W., Ettinger, G. J., White, S., Gleason, P., Lozano-Perez, T., W. M. Wells, I., & Kikinis, R. (1995). Evaluating and validating an automated registration system for enhanced reality visualization in surgery. *Proceedings of the IEEE First International Conference on Computer Vision, Virtual Reality and Robotics in Medicine (CVRMed'95),* 3–12.

Henri, C. J., Colchester, A., Zhao, J., Hawkes, D., Hill, D., & Evans, R. L. (1995). Registration of 3D surface data for intra-operative guidance and visualization in frameless stereotactic neurosurgery. *Proceedings of the IEEE First International Conference on Computer Vision, Virtual Reality and Robotics in Medicine (CVRMed'95),* 47–58.

Holloway, R. (1994). *An analysis of registration errors in a see-through head-mounted display system for craniofacial surgery planning*. Unpublished doctoral dissertation, University of North Carolina at Chapel Hill.

Holloway, R. L. (1997). Registration error analysis for augmented reality. *Presence: Teleoperators and Virtual Environments, 6*(4), 413–432.

Janin, A., Mizell, D., & Caudell, T. (1993). Calibration of head-mounted displays for augmented reality applications. *Proceedings of the Virtual Reality Annual Symposium (VRAIS'93),* 246–255.

Kancherla, A. R., Rolland, J. P., Wright, D. L., & Burdea, G. (1995). A novel virtual reality tool for teaching dynamic 3D anatomy. *Proceedings of the IEEE First International Conference on Computer Vision, Virtual Reality and Robotics in Medicine (CVRMed'95),* 163–169.

Kato, H., & Billinghurst, M. (1999). Marker tracking and HMD calibration for a video-based augmented reality conferencing system. *Proceedings of the 2nd IEEE and ACM International Workshop on Augmented Reality (IWAR'99),* 85–94.

Koller, D., Klinker, G., Rose, E., Breen, D., Whitaker, R., & Tuceryan, M. (1997). Real-time vision-based camera tracking for augmented reality applications. *Proceedings of the Symposium on Virtual Reality Software and Technology (VRST-97),* 87–94.

Kutulakos, K. N., & Vallino, J. R. (1996). Affine object representations for calibration-free augmented reality. *Proceedings of the Virtual Reality Annual Symposium (VRAIS'96),* 25–36.

Lenz, R. K., & Tsai, R. (1988). Techniques for calibration of the scale factor and image center for high accuracy 3D machine vision metrology. *IEEE Trans. on Pattern Analysis and Machine Intelligence, 10*(5), 713–720.

Maybank, S. J., & Faugeras, O. D. (1992). A theory of self-calibration of a moving camera. *International Journal of Computer Vision, 8*(2), 123–151.

McGarrity, E., & Tuceryan, M. (1999). A method for calibrating see-through head-mounted displays for AR. *Proceedings of the 2nd IEEE and ACM International Workshop on Augmented Reality (IWAR'99),* 75–84.

Mellor, J. P. (1995). Real-time camera calibration for enhanced reality visualizations. *Proceedings of the IEEE First International Conference on Computer Vision, Virtual Reality and Robotics in Medicine (CVRMed'95),* 471–475.

Nagata, S. (1991). How to reinforce perception of depth in single two-dimensional pictures. In S. R. Ellis (Ed.), *Pictorial Communication in Virtual and Real Environments,* 2nd ed. (pp. 527–545). London: Taylor & Francis Ltd.

Navab, N., Bani-Hashemi, A., Nadar, M. S., Wiesent, K., Durlak, P., Brunner, T., Barth, K., & Graumann, R. (1998). 3D reconstruction from projection matrices in a C-arm based 3D-angiography system. *First International Conference on Medical Image Computing and Computer Assisted Intervention (MICCAI),* 119–129.

Neumann, U., & Cho, Y. (1996). A self-tracking augmented reality system. *Proceedings of the ACM Symposium on Virtual Reality and Applications,* 109–115.

Peria, O., Chevalier, L., François-Joubert, A., Caravel, J. P., Dalsoglio, S., Lavallee, S., & Cinquin, P. (1995). Using a 3D position sensor for registration of SPECT and US images of the kidney. *Proceedings of the IEEE First International Conference on Computer Vision, Virtual Reality and Robotics in Medicine (CVRMed'95),* 23–29.

Sauer, F., Wenzel, F., Vogt, S., Tao, Y., Genc, Y., & Bani-Hashemi, A. (2000). Augmented workspace: Designing an AR testbed. *Proceedings of the IEEE and ACM First International Symposium on Augmented Reality (ISAR'00),* 47–53.

State, A., Hirota, G., Chen, D. T., Garrett, W. F., & Livingston, M. A. (1996). Superior augmented reality registration by integrating landmark tracking and magnetic tracking. *Proceedings of the 23rd Annual Conference on Computer Graphics,* 429–438.

Trucco, E., & Verri, A. (1998). *Introductory techniques for 3D computer vision.* Upper Saddle River, NJ: Prentice-Hall.

Tuceryan, M., Greer, D., Whitaker, R., Breen, D., Crampton, C., Rose, E., & Ahlers, K. (1995). Calibration requirements and procedures for a monitor-based augmented reality system. *IEEE Transactions on Visualization and Computer Graphics, 1*(3), 255–273.

Uenohara, M., & Kanade, T. (1995). Vision-based object registration for real-time image overlay. *Proceedings of the IEEE First International Conference on Computer Vision, Virtual Reality and Robotics in Medicine (CVRMed'95),* 13–22.

Weng, J., Cohen, P., & Herniou, M. (1992). Camera calibration with distortion models and accuracy evaluation. *IEEE Trans. on Pattern Analysis and Machine Intelligence, 14*(10), 965–980.